© 2014. Published by The Company of Biologists Ltd | Development (2014) 141, 4548-4557 doi:10.1242/dev.109538

RESEARCH ARTICLE

Regulation of synaptic development and function by the *Drosophila* PDZ protein Dyschronic

James E. C. Jepson[1,2,*], Mohammed Shahidullah[1,*], Die Liu[1,‡], Sylvain J. le Marchand[1,‡], Sha Liu[3], Mark N. Wu[3], Irwin B. Levitan[1], Matthew B. Dalva[1] and Kyunghee Koh[1,§]

ABSTRACT

Synaptic scaffold proteins control the localization of ion channels and receptors, and facilitate molecular associations between signaling components that modulate synaptic transmission and plasticity. Here, we define novel roles for a recently described scaffold protein, Dsychronic (DYSC), at the *Drosophila* larval neuromuscular junction. DYSC is the *Drosophila* homolog of whirlin/DFNB31, a PDZ domain protein linked to Usher syndrome, the most common form of human deaf-blindness. We show that DYSC is expressed presynaptically and is often localized adjacent to the active zone, the site of neurotransmitter release. Loss of DYSC results in marked alterations in synaptic morphology and cytoskeletal organization. Moreover, active zones are frequently enlarged and misshapen in *dysc* mutants. Electrophysiological analyses further demonstrate that *dysc* mutants exhibit substantial increases in both evoked and spontaneous synaptic transmission. We have previously shown that DYSC binds to and regulates the expression of the Slowpoke (SLO) BK potassium channel. Consistent with this, *slo* mutant larvae exhibit similar alterations in synapse morphology, active zone size and neurotransmission, and simultaneous loss of *dysc* and *slo* does not enhance these phenotypes, suggesting that *dysc* and *slo* act in a common genetic pathway to modulate synaptic development and output. Our data expand our understanding of the neuronal functions of DYSC and uncover non-canonical roles for the SLO potassium channel at *Drosophila* synapses.

KEY WORDS: PDZ domain, Scaffold protein, Active zone, BK channel, *Drosophila*, Neuromuscular junction

INTRODUCTION

Elucidating the molecular mechanisms of synapse development and function is important for understanding biological processes such as learning and memory, as well as neurological diseases such as autism spectrum disorder and schizophrenia (Caroni et al., 2012; Sudhof, 2008; Wondolowski and Dickman, 2013). Crucial to correct synaptic organization are scaffold proteins, which act as organizing hubs that link ion channels, neurotransmitter receptors and other membrane proteins to the cytoskeleton and to downstream intracellular signaling networks (Emes and Grant, 2012; Verpelli et al., 2012). In a screen for *Drosophila* with altered circadian behavior, we recently identified a previously uncharacterized gene encoding a scaffold protein with multiple PDZ domains that we termed *dyschronic* (*dysc*). Loss of DYSC results in arrhythmic patterns of circadian locomotor activity, and *dysc* is the *Drosophila* homolog of the human locus *whirlin/DFNB31*, mutations in which lead to Usher syndrome (USH), a leading cause of deaf-blindness (Jepson et al., 2012; Mburu et al., 2003). We found that DYSC binds to and controls the expression of the Slowpoke (SLO) BK potassium channel in the adult *Drosophila* nervous system, thus identifying DYSC as a novel ion channel regulator that impacts complex behavior (Jepson et al., 2012).

BK potassium channels are synergistically activated by membrane depolarization and elevated intracellular Ca^{2+} (Barrett et al., 1982; Lee and Cui, 2010; Prakriya and Lingle, 1999). In neurons, BK channels limit action potential duration by linking Ca^{2+} influx through voltage-gated Ca^{2+} channels (VGCCs) to potassium efflux (Bean, 2007). Interestingly, in addition to the axon, BK channels are also localized at the synapse near to the active zone (AZ) (Hu et al., 2001), a crucial structural determinant of the probability of vesicle fusion (Sigrist and Schmitz, 2011). In *Drosophila*, the AZ is an electron-dense macromolecular structure and functions in part to tether synaptic vesicles in close proximity to VGCCs (Atwood et al., 1993; Koenig and Ikeda, 1999); recent genetic studies have uncovered a number of core constituents of the *Drosophila* AZ as well as proteins involved in its assembly (Johnson et al., 2009; Kaufmann et al., 2002; Kittel et al., 2006; Liu et al., 2011; Nieratschker et al., 2009; Wagh et al., 2006). For example, Bruchpilot (BRP) is a key component of T-bars, dense bodies that project intracellularly from the AZ core and connect to a subpopulation of synaptic vesicles (Atwood et al., 1993; Koenig and Ikeda, 1999; Reist et al., 1998; Wagh et al., 2006). Using super-resolution microscopy, BRP complexes have been shown to form donut-like rings around a central core of VGCCs, and loss of BRP results in reduced VGCC localization in the AZ and a substantial decrease in evoked excitatory currents (Kittel et al., 2006). However, whereas much research has focused on molecules that promote AZ formation and neurotransmitter release, less is known regarding factors that negatively regulate the AZ and vesicle fusion.

Here, we demonstrate that DYSC and SLO coordinately influence diverse aspects of synaptic development and function at the *Drosophila* larval neuromuscular junction (NMJ), and act as negative regulators of AZ size and evoked neurotransmission. Most surprisingly, spontaneous vesicle fusion is enhanced in *dysc* and *slo* mutants, even in zero-Ca^{2+} conditions, suggesting that SLO channels impact spontaneous neurotransmission independently of enhanced VGCC activity. Our results reveal intriguing non-canonical roles for the SLO BK channel and significantly expand the known functions of the USH homolog DYSC in the *Drosophila* nervous system.

[1]Department of Neuroscience, The Farber Institute for Neurosciences, Thomas Jefferson University, Philadelphia, PA 19107, USA. [2]UCL Institute of Neurology, London WC1N 3BG, UK. [3]Department of Neurology, John Hopkins University, Baltimore, MD 21287, USA.
*These authors contributed equally to this work
‡These authors contributed equally to this work

§Author for correspondence (kyunghee.koh@jefferson.edu)

Received 26 February 2014; Accepted 16 September 2014

Development (2014) 141, 4548-4557 doi:10.1242/dev.109538

RESULTS

DYSC regulates synaptic morphology and cytoskeletal organization

We have previously found that DYSC is broadly localized within the adult fly brain and exhibits strong expression in axonal tracts throughout the nervous system (Jepson et al., 2012). However, DYSC is also present in synaptic neuropil regions (Jepson et al., 2012). We were therefore intrigued by the possibility that DYSC might play important roles at *Drosophila* synapses.

To test whether DYSC regulates synaptic development and/or function, we turned to the NMJ of third instar *Drosophila* larvae, a model glutamatergic synapse, the structural and functional properties of which have been extensively studied. We initially examined synaptic morphology of *dysc* mutants using two transposon insertion alleles ($dysc^{c03838}$ and $dysc^{s168}$) (Fig. 1A). The *dysc* transcription unit generates protein isoforms containing two or three PDZ domains (Jepson et al., 2012) (Fig. 1A; www.flybase.org). Both long and short DYSC isoforms are undetectable by western blotting of $dysc^{c03838}$ head extracts (Jepson et al., 2012), and *dysc* cDNA expression was not detected in $dysc^{c03838}$ head tissue (supplementary material Fig. S1A), indicating that $dysc^{c03838}$ is a null allele. By contrast, the $dysc^{s168}$ insertion selectively disrupts expression of long DYSC isoforms containing three PDZ domains, while leaving the short isoform intact (Jepson et al., 2012).

Both $dysc^{c03838}$ and $dysc^{s168}$ homozygotes exhibited a ~40% reduction in the total number of synaptic boutons at muscle 6/7 (Fig. 1B,C), resulting from a decrease in the number of both type 1b and type 1s boutons (supplementary material Fig. S1B,C). A similar phenotype was observed in $dysc^{c03838}/dysc^{s168}$ trans-heterozygotes, but there was no significant alteration in bouton number in $dysc^{c03838}/+$ or $dysc^{s168}/+$ heterozygotes (Fig. 1B,C; supplementary material Fig. S1B,C). *dysc* homozygous and trans-heterozygous mutants also exhibited a substantial increase in the average size of type 1b boutons (Fig. 1B,D). By contrast, mean synaptic area and branch number were not altered in *dysc* mutants (supplementary material Fig. S1D,E). Similar phenotypes in terms of bouton number and size were observed in larval synapses innervating muscle 4 (supplementary material Fig. S1F,G). Thus, DYSC regulates the number and size of larval synaptic boutons but not overall synaptic size.

Because whirlin, the mammalian DYSC homolog, has recently been shown to affect the stability of the axonal cytoskeleton (Green et al., 2013), we wondered whether DYSC modulates synaptic morphology by controlling the localization of synaptic cytoskeletal proteins. We therefore visualized expression of the microtubule-binding protein Futsch in wild-type and *dysc* mutant synapses (Fig. 1E). Futsch-mediated regulation of microtubule organization is important for correct synaptic bouton budding (Roos et al., 2000), and mislocalization of synaptic Futsch in various *Drosophila* mutants has been associated with reduced synaptic bouton number and increased bouton size (Mosca et al., 2012; Pennetta et al., 2002). Consistent with previous data (Roos et al., 2000), filamentous 'tendrils' and structured 'loops' of Futsch-bound microtubules were generally observed in wild-type synapses (Fig. 1E). By contrast, ~25% of *dysc* mutant synapses exhibited an abnormal mode of Futsch localization, characterized by a substantially increased level of unstructured Futsch within synaptic boutons (Fig. 1E,F; supplementary material Fig. S2). This pattern of Futsch expression was rarely observed in wild-type synaptic boutons (~2.6%, Fig. 1F). Thus, loss of DYSC leads to an alteration in the synaptic localization of a key cytoskeletal regulator in a manner consistent with an inhibition of synaptic bouton budding in *dysc* mutants.

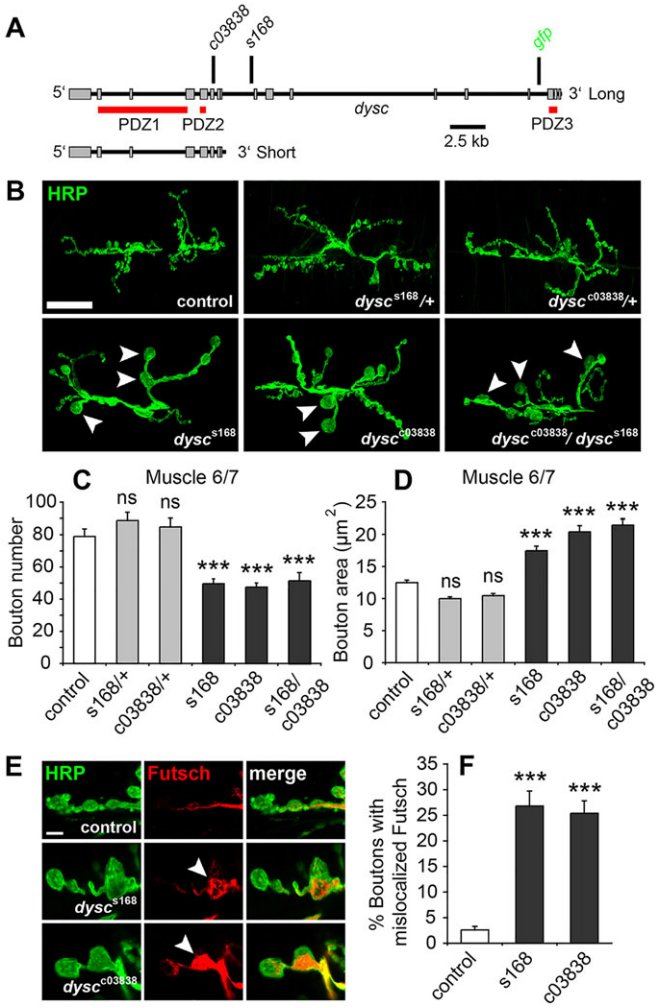

Fig. 1. DYSC regulates synaptic morphology and Futsch localization. (A) Schematic of the *dysc* transcription unit, locations of the $dysc^{c03838}$ and $dysc^{s168}$ P-element insertions and the MiMIC protein trap insertion used to generate the *dysc::gfp* allele. Genomic regions encoding the three PDZ domains are also shown. (B) Confocal projections showing representative NMJs at muscle 6/7, segment 3. Neuronal membranes are labeled with anti-HRP. Arrowheads indicate enlarged synaptic boutons in $dysc^{s168}$ and $dysc^{c03838}$ homozygotes that are absent in controls or heterozygotes. Scale bar: 20 µm. (C,D) Average number of total synaptic boutons (C) and average bouton size (D) in wild-type controls, and in $dysc^{s168}$ and $dysc^{c03838}$ heterozygotes and homozygotes, and $dysc^{c03838}/dysc^{s168}$ trans-heterozygotes. (C) *n*=12-29 synapses. (D) *n*=167-211 boutons. (E) Confocal slices illustrating localization of Futsch in synaptic termini in wild-type controls and $dysc^{s168}$ and $dysc^{c03838}$ homozygotes. Arrowheads indicate synaptic boutons exhibiting unusual unbundled accumulation of Futsch. Scale bar: 5 µm. (F) Quantification of the mean proportion of boutons exhibiting unbundled Futsch. *n*=14-16 synapses, 265-381 boutons. Values represent mean±s.e.m. ***P<0.0005; ns, not significant (P>0.05), one-way ANOVA with Dunnett post-hoc test.

DYSC localizes to synaptic termini and is required presynaptically

We next sought to examine the localization of DYSC at the larval NMJ. Immunohistochemical experiments using our previously described anti-DYSC antibody failed to generate robust signals at larval synapses, possibly due to low efficacy and/or low DYSC expression. To make use of a higher affinity antibody, we used the MiMIC system (Venken et al., 2011) to insert a GFP/FlASH/StrepII/3xFLAG protein trap upstream of the region encoding the

Development (2014) 141, 4548-4557 doi:10.1242/dev.109538

third PDZ domain (Fig. 1A). This strategy allowed labeling of DYSC isoforms containing three PDZ domains using anti-GFP and anti-FLAG antibodies. We term this new *dysc* allele *dysc::gfp*.

The protein trap exon does not disrupt the PDZ domain-coding sequences within the *dysc* locus, and importantly, *dysc::gfp* larvae exhibited normal synaptic morphology (supplementary material Fig. S3A-C). Furthermore, *dysc::gfp* adult flies exhibited rhythmic patterns of circadian locomotion under constant-dark conditions (data not shown). Thus, the GFP insertion does not inhibit the normal function of DYSC.

In both the adult and the larval *Drosophila* nervous systems, GFP-tagged DYSC was localized to axonal regions and, importantly, to the synaptic neuropil, as evidenced by colocalization with the presynaptic marker Bruchpilot (BRP) (Kittel et al., 2006; Wagh et al., 2006) (supplementary material Fig. S3D,E). At the larval NMJ, full-length DYSC detected using an anti-GFP antibody exhibited a punctate pattern of localization in both motor neuron axon bundles and in synaptic bouton termini (Fig. 2A). A similar expression pattern was observed when using an anti-FLAG antibody to detect DYSC (supplementary material Fig. S4A), and this pattern was not observed in larvae lacking the *dysc::gfp* allele using either anti-GFP (Fig. 2A) or anti-FLAG antibodies (supplementary material Fig. S4A). Furthermore, neuronal overexpression of a long DYSC isoform in combination with an anti-DYSC antibody generated similar presynaptic punctate signals (supplementary material Fig. S4B,C).

The localization of DYSC::GFP suggested a presynaptic function for DYSC. Consistent with this hypothesis, pre- but not postsynaptic expression of a full-length DYSC transgene (*uas-dysc-long*) significantly rescued both the reduced bouton number and increased bouton size of *dysc* mutants (Fig. 2B-D). Transgenic restoration of DYSC solely in neurons also rescued the mislocalization of synaptic Futsch (supplementary material Fig. S5).

The similar phenotypes of $dysc^{c03838}$ and $dysc^{s168}$ homozygotes further suggested that full-length DYSC isoforms containing three PDZ domains are specifically required for normal synaptic bouton proliferation, as expression of the short DYSC isoform containing the two N-terminal PDZ domains is maintained at wild-type levels in $dysc^{s168}$ homozygotes (Jepson et al., 2012). We therefore performed rescue experiments using a transgene encoding a short DYSC isoform (*uas-dysc-short*), and indeed found that neither neuronal nor muscle expression of the short DYSC isoform rescued any aspect of synaptic morphology (Fig. 2C,D).

In addition, to test whether DYSC levels influence synaptic bouton size and number in a dose-dependent manner, we overexpressed DYSC in neurons in a wild-type background. Overexpression of either long or short DYSC transgenes did not alter bouton number or size relative to controls (supplementary material Fig. S6). These experiments indicate that DYSC is required in the presynaptic compartment to influence synaptic development, and suggest that the C-terminal region that includes the third PDZ domain of DYSC is required for this function.

DYSC influences the architecture of active zones

We next sought to examine the subcellular localization of presynaptic DYSC puncta in more detail by immunostaining synapses in *dysc::gfp* larvae with anti-GFP and either anti-Bruchpilot (anti-BRP) or anti-Fasciclin II (FASII) antibodies.

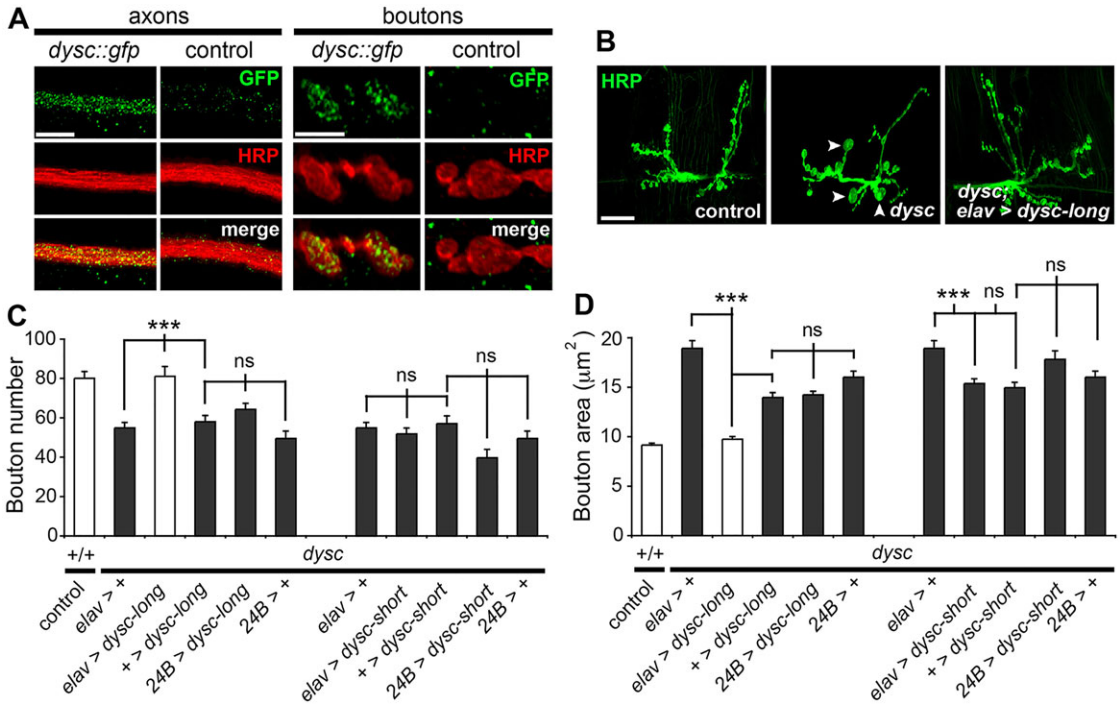

Fig. 2. DYSC is required in neurons for correct synaptic development. (A) Confocal slices illustrating punctate expression of DYSC::GFP (GFP) in both axonal bundles descending from the larval ventral nerve cord and at synaptic bouton termini. This staining pattern was not observed in controls lacking the *dysc::gfp* insertion. Scale bars: 20 μm in axons; 5 μm in boutons. (B) Confocal projections showing representative NMJs at muscle 6/7, segment 3 of wild-type controls, $dysc^{c03838}$ (*dysc*) homozygotes and *dysc* larvae with presynaptic expression of a *uas-dysc-long* transgene. Neuronal membranes are labeled with anti-HRP. Arrowheads indicate enlarged synaptic boutons in *dysc* larvae that are absent following presynaptic restoration of full-length DYSC. Scale bar: 20 μm. (C,D) Pre- and postsynaptic rescue experiments examining bouton number (C; *n*=12-20) or bouton size (D; *n*=176-326) using either *elav*-Gal4 (neurons) or *24B*-Gal4 (muscle) drivers to express short or long DYSC isoforms. For ease of viewing, the data for *elav*-Gal4/+ and *24B*-Gal4/+ synapses are repeated on each side of the graph. Values represent mean±s.e.m. ***P<0.0005; ns, not significant (P>0.05), one-way ANOVA with Tukey's post-hoc test.

Development (2014) 141, 4548-4557 doi:10.1242/dev.109538

BRP is a key constituent of T-bars, electron-dense protrusions found at the AZ (Kittel et al., 2006; Wagh et al., 2006), whereas FASII is a marker for periactive zones linked to endocytosis (Sone et al., 2000). DYSC::GFP puncta were often (but not always) adjacent to or overlapping with BRP-labeled T-bars (Fig. 3A, upper panel). Transgenic full-length DYSC expressed presynaptically exhibited a similar localization near BRP puncta (supplementary material Fig. S4C). By contrast, DYSC::GFP exhibited little overlap with FASII (Fig. 3A, lower panel), indicating that synaptic DYSC is preferentially localized in close proximity to AZs.

Given the close association of DYSC and BRP-labeled T-bars, we next investigated whether DYSC influences the expression or localization of BRP. Under confocal microscopy, we observed no clear alteration either in the localization of BRP or the apposition between BRP and the postsynaptic Glutamate Receptor IIC (GLURIIC) in *dysc* mutant synapses (supplementary material Fig. S7A,B), nor any significant change in GLURIIC levels (supplementary material Fig. S7B,C). However, at increased magnification, the size of BRP puncta appeared to be somewhat increased in *dysc* mutants (supplementary material Fig. S7B).

These observations suggested that DYSC might impact the fine structure of T-bars. We therefore used a super-resolution imaging technique, stimulated emission depletion (STED) microscopy (Dyba et al., 2003), to obtain nanometer-scale images of BRP structures wild-type and *dysc* mutant synapses (Fig. 3B). As shown previously (Kittel et al., 2006; Liu et al., 2011; Owald et al., 2012), BRP forms donut-like structures in wild-type synapses when observed under STED imaging (Fig. 3B). Intriguingly, we found that both $dysc^{c03838}$ homozygous and $dysc^{c03838}/dysc^{s168}$ trans-heterozygous mutants exhibited a significant increase in the mean area of individual BRP rings (Fig. 3B,C). Furthermore, we observed frequent merging of neighboring BRP rings in *dysc* mutants (Fig. 3B). These phenotypes were rescued by neuronal expression of a full-length DYSC transgene, confirming that this phenotype is caused by a loss of presynaptic DSYC (Fig. 3D,E). Thus, in addition to modulating synaptic morphology, DYSC also plays a significant role in regulating the macromolecular architecture of a key constituent of the AZ.

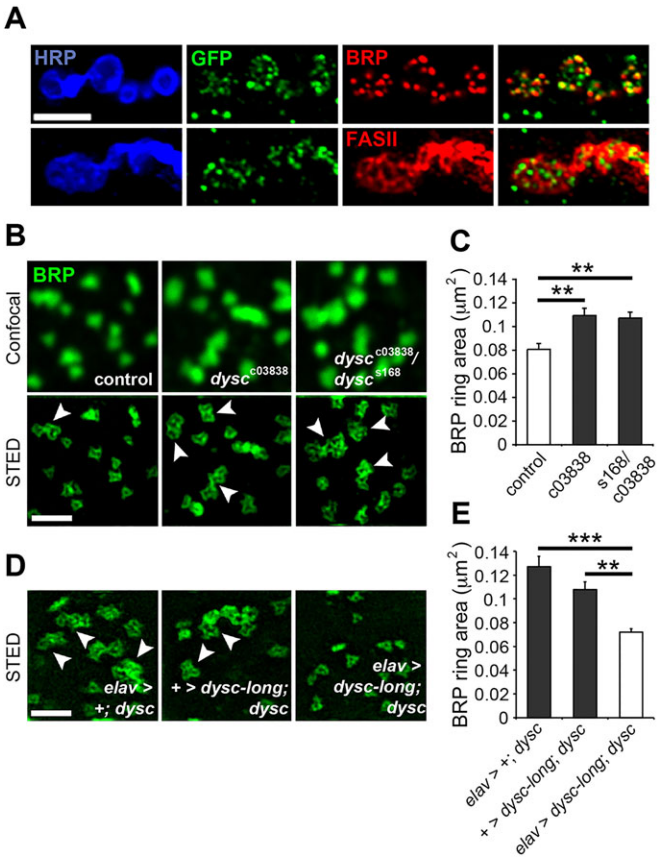

Fig. 3. DYSC modulates the structural composition of active zones. (A) Confocal slices illustrating subcellular localization of DYSC::GFP (GFP) in the presynaptic compartment. DYSC::GFP puncta are often closely associated with the AZ component Bruchpilot (BRP, upper panel). By contrast, there is little overlap between DYSC::GFP and the periactive zone marker FASII (lower panel). Scale bar: 5 µm. (B) Representative confocal (top) and STED (bottom) slices of BRP-marked AZs in control larvae and two *dysc* allelic backgrounds. Arrowheads indicate clustered AZs. Scale bar: 1 µm. (C) Average area for individual AZs in control and *dysc* mutant synapses. *n*=39-56 AZs. (D) Representative STED images of AZ organization in $dysc^{c03838}$ (*dysc*) mutants harboring the pan-neuronal *elav*-Gal4 (*elav*) driver, a *uas-dysc-long* transgene (*dysc-long*) or both. Arrowheads indicate clustered AZs. Scale bar: 1 µm. (E) Average area of individual AZs in the above genotypes. Values represent mean±s.e.m. *n*=29-57 AZs. ***P*<0.005; ****P*<0.0005, one-way ANOVA with Dunnett post-hoc test.

SLO channels impact synaptic development at the larval NMJ

We have previously shown that DYSC binds to and promotes the expression of SLO channels in the adult *Drosophila* nervous system (Jepson et al., 2012). However, whether this is also the case at earlier developmental time points is unclear. Consistent with our previous data in the adult brain, loss of DYSC also resulted in a robust reduction in SLO expression in motor neuron axons of the larval ventral nerve cord (supplementary material Fig. S8A). Previous work has shown that mutations in *slo* lead to an increased frequency of rhythmic peristalsis of the body wall muscle (McKiernan, 2013), and, similarly, we found that larvae homozygous for both $dysc^{s168}$ and $dysc^{c03838}$ also exhibited a significant enhancement in the rate of peristalsis (supplementary material Fig. S8B).

We next asked whether the alterations in synaptic bouton morphology found in *dysc* mutants were also observed in larvae lacking SLO channels. To this end, we obtained a *slo* mutant line carrying a Minos element insertion in the exon encoding transmembrane domain 2 of the SLO channel (slo^{11481}; www.flybase.org), resulting in an interruption in the coding sequence that is expected to inhibit production of full-length *slo* transcripts, and examined how this mutation affects synaptic development. We confirmed that, as predicted, slo^{11481} is a null allele using RT-PCR (supplementary material Fig. S9A). In addition, to control for differences in genetic background, we outcrossed all *dysc* and *slo* alleles into an isogenic $white^{1118}$ (*iso*31) background for 5-10 generations.

Like *dysc* mutants, slo^{11481} larval synapses exhibited significantly increased bouton areas (Fig. 4A,C). This phenotype was also observed in genetic backgrounds containing trans-heterozygotic combinations of slo^{11481}, slo^{4} (a canonical *slo* null allele resulting from a large chromosomal inversion), slo^{1} (a null or strongly hypomorphic allele) and slo^{Df} (a deficiency removing the *slo* locus) (supplementary material Fig. S9B,D,F), and was rescued by the introduction of a *slo* transgene (Fig. 4C) (Ghezzi et al., 2004).

Interestingly, in contrast to *dysc* mutants, synaptic bouton number was not significantly altered in any of the *slo* mutants we examined (Fig. 4B and supplementary material Fig. S9C,E). This contrasts with previous work reporting that larvae homo- or transheterozygous for three *slo* alleles (slo^{1}, slo^{98} and slo^{4}) exhibit a hyper-budding phenotype at larval synapses (Lee and Wu, 2010). Our experiments

Development (2014) 141, 4548-4557 doi:10.1242/dev.109538

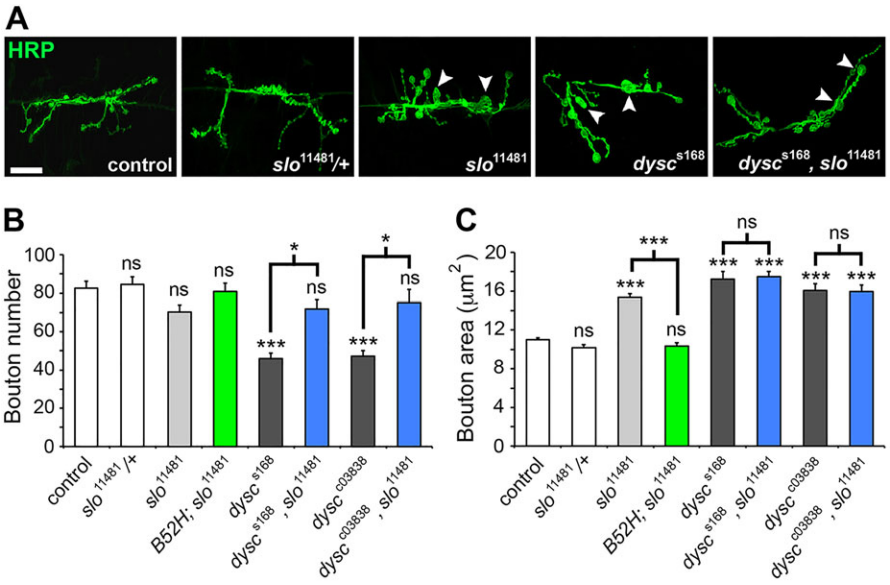

Fig. 4. *slo* and *dysc* act in the same pathway to regulate synaptic bouton morphology. (A) Representative confocal projections of synapses from control larvae, slo^{11481} heterozygotes and homozygotes, $dysc^{s168}$ homozygotes, and $dysc^{s168}$, slo^{11481} double mutants labeled with anti-HRP. Arrowheads indicate enlarged boutons that are present in slo^{11481} and $dysc^{s168}$ homozygotes, as well as $dysc^{s168}$, slo^{11481} double mutants. Scale bar: 20 µm. (B,C) Average bouton number (B) and bouton area (C) in wild-type controls, slo^{11481} heterozygotes, *slo* and *dysc* homozygotes, *dysc, slo* double mutants, and slo^{11481} homozygotes harboring a *slo* rescue construct (*B52H*). *n*=10-40 synapses and 195-463 boutons. Values represent mean±s.e.m. **P*<0.05; ****P*<0.0005; ns, not significant (*P*>0.05), one-way ANOVA with Tukey's post-hoc test.

were performed at 25°C in an *iso*31 genetic background, whereas the previous analysis was performed at room temperature in a Canton-S background (Lee and Wu, 2010). Phenotypic effects of mutations may be modified by both environmental conditions and genetic background (Chari and Dworkin, 2013; Dworkin et al., 2009; Wang et al., 2014). Indeed, of the three *slo* mutants we examined raised at a lower temperature of 18°C (slo^{11481} and slo^{4} homozygotes, and slo^{1}/slo^{4} transheterozygotes), only slo^{4} homozygotes exhibited a measurable increase in synaptic bouton budding (supplementary material Fig. S10). The slo^{4} chromosome contains a large inversion that prevents recombination, and it is likely that despite being outcrossed to an *iso*31 background five times, slo^{4} retains a substantial amount of the original background. Thus, slo^{4} mutants may harbor additional mutations that impact synaptic development in a temperature-sensitive manner. We conclude that in an *iso*31 genetic background, SLO channels predominantly act to negatively regulate bouton size rather than suppressing synaptic bouton budding.

dysc and *slo* act in a common genetic pathway to regulate synaptic bouton morphology

To examine whether *slo* and *dysc* are components of the same genetic pathway, we generated *slo, dysc* double mutants using two independent alleles of *dysc* and the slo^{11481} allele, and compared their synaptic phenotype relative to individual *slo* and *dysc* mutations. In relation to bouton size, *slo, dysc* double mutants exhibited significantly increased bouton size relative to controls ($P<0.0001$), but were not significantly different when compared with *dysc* mutations alone ($P>0.99$, one-way ANOVA with Tukey's post-hoc test) (Fig. 4B,D). Furthermore, we observed a significant increase in bouton size in $slo^{11481}/dysc^{c03838}$ transheterozygotes relative to controls and heterozygotes for either allele (supplementary material Fig. S9G), demonstrating a synergistic interaction between the two genes.

Unexpectedly, we found that loss of SLO suppressed the reduction in synaptic bouton number observed in *dysc* mutants (Fig. 4B,C). A number of mechanisms could account for this effect. For example, loss of DYSC may lead to an altered subcellular localization of SLO that results in reduced bouton number, which is rescued by complete loss of SLO. Alternatively, selective loss of SLO in neurons but not in muscle tissue in *dysc* mutants may affect bouton number, whereas complete loss of SLO does not. We were unable to test these competing hypotheses because synaptic SLO could not be detected using our previously described antibody (Jepson et al., 2012) or a SLO::GFP fusion generated using the MiMIC system (Venken et al., 2011) (data not shown). Nonetheless, the genetic interactions between *dysc* and *slo* alleles detailed above strongly suggest that DYSC and SLO act in a common pathway to influence synaptic bouton size and number.

SLO channels impact active zone structure and Futsch localization

As *dysc* mutants display alterations in the structure of a key AZ complex, we determined whether *slo* mutants also exhibit similar AZ defects. Under STED microscopy, larvae homozygous for the slo^{11481} allele indeed exhibited an increase in BRP ring area and clustering that was almost identical to that seen in *dysc* larvae (Fig. 5). Larvae lacking a distinct potassium channel, Shaker, did not exhibit either an increase in BRP area or merging of BRP rings, suggesting that the alterations in AZ structure in *slo* mutants are not due to a general effect of neuronal hyperexcitability (supplementary material Fig. S11).

To test whether SLO and DYSC act in the same pathway for the regulation of AZ morphology, we visualized BRP rings in *dysc, slo* double mutants. The phenotype of *dysc, slo* double mutants was statistically indistinguishable from each individual mutation (Fig. 5A,B; $P>0.27$, one-way ANOVA with Tukey's post-hoc test), suggesting that DYSC and SLO act in the same pathway to regulate AZ size. Furthermore, we also observed a mislocalization of synaptic Futsch in *slo* mutants similar to that observed following loss of DYSC (supplementary material Fig. S12). Collectively, the above data provide evidence that DYSC and SLO act in a common pathway to regulate synaptic morphology, cytoskeletal dynamics and presynaptic macromolecular organization.

DYSC and SLO inhibit evoked neurotransmission

To test whether DYSC also impacts the physiology of larval synapses, we recorded evoked excitatory junctional currents (EJCs) in muscle 6/7 under voltage-clamp mode. We observed a significant increase in both the EJC amplitude and width in $dysc^{c03838}$ larvae relative to controls (Fig. 6A-C). The enhancement of the EJC amplitude was rescued by presynaptic expression of a full-length DYSC transgene in $dysc^{c03838}$ homozygotes (Fig. 6D,E), and there

Development (2014) 141, 4548-4557 doi:10.1242/dev.109538

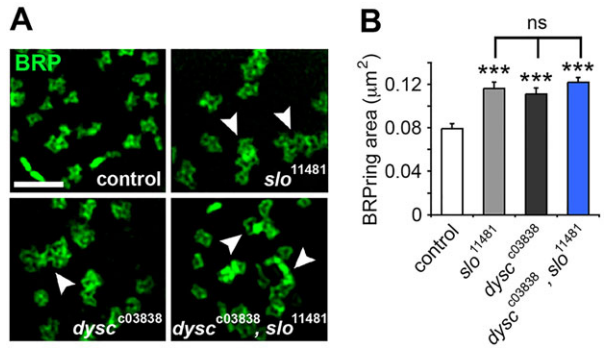

Fig. 5. DYSC and SLO act in concert to regulate AZ structure. (A) Representative STED slices of BRP-labeled AZs in wild-type control, individual *slo*^{11481} and *dysc*^{c03838} homozygotes, and *dysc*^{c03838}, *slo*^{11481} double mutant larval synapses. Scale bar: 1 µm. Arrowheads indicate clustered AZs. (B) Average BRP ring area for the above genotypes. Values represent mean±s.e.m. *n*=40-52 AZs; ns, not significant (*P*>0.05), ***P*<0.0005, one-way ANOVA with Tukey's post-hoc test.

was a trend towards a rescue of the increased EJC width in the same genetic background (Fig. 6F). Thus, presynaptic DYSC negatively regulates evoked synaptic transmission.

The larger and broader action potentials in *dysc* mutants would be predicted to result in higher concentrations of intracellular Ca^{2+}. As the levels of intracellular Ca^{2+} near the sites of neurotransmitter release influence the probability of vesicle fusion (Katz and Miledi, 1963), we examined whether *dysc* mutants also exhibited alterations in short-term synaptic plasticity using a paired-pulse protocol. Consistent with previous data (Kittel et al., 2006), paired EJCs from wild-type NMJs were approximately constant over an interval of 30-130 ms (supplementary material Fig. S13). By contrast, EJCs from *dysc* mutant NMJs exhibited significant paired-pulse facilitation over this interval (supplementary material Fig. S13). Thus, in addition to altering the basal properties of evoked currents, DYSC also regulates short-term plasticity.

As DYSC promotes neuronal SLO channel expression (Jepson et al., 2012), we also tested whether DYSC and SLO act in the same genetic pathway to regulate evoked synaptic transmission by examining evoked currents in *slo* and *dysc, slo* double mutants (Fig. 6A-C). Similar, to *dysc* mutants, *slo* mutants exhibited a significant increase in EJC amplitude and width (Fig. 6A-C). This contrasts with previous studies that reported no significant alterations of EJC amplitudes in *slo* mutants (Lee et al., 2008, 2014), but these discrepancies may due to different genetic backgrounds as discussed above. Importantly, *dysc, slo* double mutants also exhibited increased EJC amplitude and width, and did not show enhanced phenotypes over single mutants (Fig. 6A-C), suggesting that DYSC and SLO act within the same pathway to negatively control evoked synaptic output.

DYSC and SLO inhibit spontaneous neurotransmitter release via a Ca^{2+}-independent mechanism

We next asked whether DYSC also modulates spontaneous vesicle fusion by examining miniature excitatory junctional currents (mEJCs) from control and *dysc*^{c03838} homozygotes (Fig. 7A). We observed a striking (~250%) increase in the frequency of mEJCs in *dysc* mutants (Fig. 7A,B), indicating that loss of DYSC results in a substantial enhancement of the probability of spontaneous vesicle release. We also observed a similar increase in mEJC frequency in *slo*^{11481} homozygotes, and analysis of mEJCs in *dysc, slo* double mutants demonstrated that the effects of these mutations were non-additive, as there were no significant differences in mEJC frequency in any of the mutant backgrounds examined (*P*>0.9, Kruskal-Wallis test with Dunn's post-hoc test) (Fig. 7B). In addition, we observed a trend towards reduced mEJC amplitudes in *dysc* and *slo* homozygotes, as well as *dysc, slo* double mutants, but this trend only achieved significance in *slo* mutants (Fig. 7C). Thus, with regard to spontaneous neurotransmission, DYSC and SLO primarily act in a common pathway to regulate the frequency of synaptic vesicle fusion.

As both *dysc* and *slo* mutants exhibit structural alterations in AZ architecture, one simple hypothesis is that the larger (and merged)

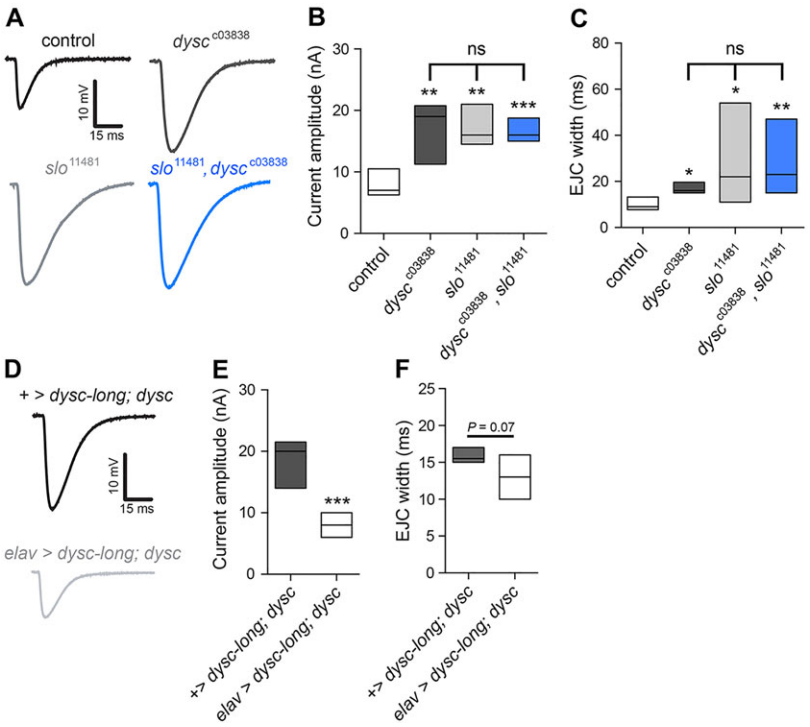

Fig. 6. DYSC and SLO inhibit evoked synaptic transmission. (A) Representative evoked excitatory junctional current (EJC) traces in wild-type control larvae, *dysc* and *slo* homozygotes, and *dysc, slo* double mutants. EJCs were measured from muscle 6/7. (B,C) Quantification of mean EJC amplitude (B) and width at 50% rise (C) in the above genotypes. *n*=7-21. (D-F) Representative EJC traces (D) and quantification of mean EJC amplitude (E) and width (F) from *dysc* mutants carrying a full-length *dysc* transgene (*uas-dysc-long*) alone or in combination with the pan-neuronal *elav*-Gal4 driver (*elav*). *n*=6-15. Data are presented as modified box plots showing the median, 25th and 75th percentiles. ns, not significant (*P*>0.05), **P*<0.05, ***P*<0.005, ****P*<0.0005, Kruskal-Wallis test with Dunn's post-hoc test (B,C) or Mann-Whitney U-test (E,F).

Development (2014) 141, 4548-4557 doi:10.1242/dev.109538

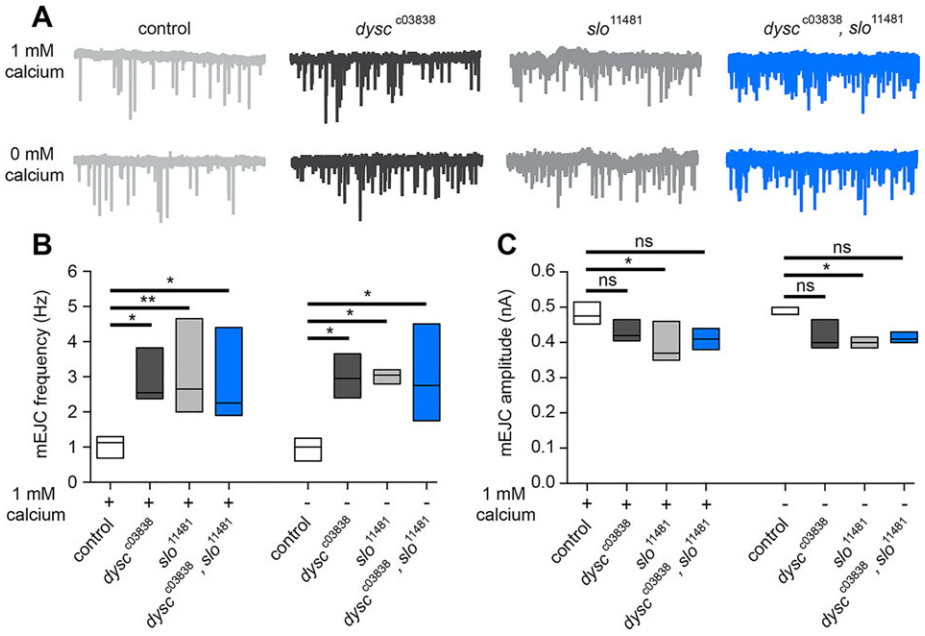

Fig. 7. DYSC and SLO inhibit spontaneous synaptic transmission independently of extracellular Ca^{2+}. (A) Representative mEJC traces illustrating spontaneous neurotransmitter release from larval presynaptic terminals in wild-type control larvae, *dysc* and *slo* homozygotes, and *dysc, slo* double mutants. (B,C) Mean mEJC frequency (B) and amplitude (C) in 1 mM (+) or 0 mM (–) extracellular Ca^{2+}. *n*=5-8 per genotype, with each data point representing the average of an individual trace. Data are presented as modified box plots showing the median, 25th and 75th percentiles. ns, not significant (*P*>0.05), **P*<0.05, ***P*<0.005, Kruskal-Wallis test with Dunn's post-hoc test.

AZs in *dysc* and *slo* mutants facilitate enhanced spontaneous vesicle fusion. The BRP ring-like complex within the AZ surrounds a central core of VGCCs (Kittel et al., 2006). Interestingly, recent work in mammalian synapses has shown that stochastic opening of VGCCs in the AZ is responsible for a substantial proportion of spontaneous neurotransmitter release (Ermolyuk et al., 2013), and that AZ size positively correlates with the frequency of spontaneous neurotransmitter release (Holderith et al., 2012; Matz et al., 2010), presumably via altered VGCC occupancy. If enhanced spontaneous vesicle fusion in *dysc* and *slo* mutants was due to an increase in the number of VGCCs within the AZ, this effect should be suppressed by removing extracellular Ca^{2+}. However, recording mEJCs in zero-Ca^{2+} saline did not alter mEJC frequency or amplitude in either control or mutant backgrounds (Fig. 7B,C). Thus, the effect of DYSC and SLO on spontaneous release is independent of voltage-gated Ca^{2+} channels and may instead be directly due to structural alterations at AZs that facilitate an increased probability of synaptic vesicle fusion.

DISCUSSION

Our work has revealed novel functions for the PDZ domain protein DYSC and its binding partner SLO in modulating diverse aspects of synaptic development and physiology, including synaptic bouton size, cytoskeletal protein localization, AZ structure and synaptic transmission. With respect to synaptic physiology, we found that DYSC acts as a negative regulator of evoked neurotransmission as well as of short-term synaptic plasticity; the alteration in evoked currents in *dysc* mutants are consistent with the known function of DYSC as a positive regulator of SLO channels (Jepson et al., 2012). Surprisingly, in addition to inhibiting evoked current amplitude and duration, DYSC and SLO also negatively regulate spontaneous neurotransmitter release in a manner that is independent of VGCC channel activation, as increased rates of miniature events are still robustly detected under zero-Ca^{2+} conditions. This finding raises the intriguing possibility that SLO channels perform non-canonical structural roles that impact spontaneous neurotransmission, as well as synaptic morphology and AZ architecture.

One issue emerging from the above results is whether altered AZ structure and spontaneous neurotransmission in *dysc* and *slo* mutants arise via a homeostatic response to increased excitability. Loss of specific ion channels in *Drosophila* has been shown to activate homeostatic transcriptional networks that act to balance excitability (Parrish et al., 2014; Ping and Tsunoda, 2012). In addition, the AZ T-bar itself has been theorized to function as a 'plasticity module' that can undergo structural adjustments in response to changes in synaptic input that, in turn, modify the probability of vesicle release (Wichmann and Sigrist, 2010). For example, at the crayfish NMJ, electrophysiological stimulation results in an increased number of AZs containing multiple T-bars (Wojtowicz et al., 1994), similar to the merged BRP rings observed in *dysc* and *slo* mutants. However, although we cannot rule out such a mechanism, we argue for a more direct role of the DYSC/SLO complex in regulating AZ formation and spontaneous neurotransmission. Numerous studies have shown that reducing postsynaptic excitability at the larval NMJ results in a compensatory increase in the probability of neurotransmitter release via a retrograde signaling mechanism (Frank et al., 2006; Muller and Davis, 2012). By contrast, in *dysc* and *slo* mutants both evoked and spontaneous neurotransmission are enhanced (Figs 6 and 7), a finding that is inconsistent with a homeostatic negative-feedback model.

Given the close proximity of DYSC to synaptic T-bars, we suggest instead that the DYSC/SLO complex directly controls AZ structure in a manner that leads to increased spontaneous vesicle fusion. Such an effect has been demonstrated for *Drosophila* Neurexin 1 (NRX-1), a synaptic cell-adhesion molecule that is also localized close to T-bars (Li et al., 2007; Owald et al., 2012). Similar to DYSC and SLO, NRX-1 negatively regulates BRP ring size and inhibits merging of BRP rings (Owald et al., 2012); these structural alterations correlate with an increased mEJP frequency in *nrx-1* mutants (Li et al., 2007). How the changes in AZ architecture observed in *dysc*, *slo* and *nrx-1* mutants are linked to enhanced rates of vesicle fusion is unclear. One possibility is that enlarged and mis-shapen AZs are less efficient at clamping synaptic vesicles to prevent premature exocytosis in the absence of Ca^{2+} (Huntwork and Littleton, 2007).

Development (2014) 141, 4548-4557 doi:10.1242/dev.109538

By what mechanisms might the DYSC/SLO complex influence AZ architecture? SLO channels contain a large intracellular C-terminal domain (Lee and Cui, 2010). Interestingly, recent studies have demonstrated that the C-terminal domain of SLACK channels, BK channel homologs that are potentiated by sodium rather than Ca^{2+}, are bound to by the Fragile-X mental retardation protein in a manner that induces channel activation (Brown et al., 2010; Zhang et al., 2012). The C-terminal domain of SLO channels may similarly act as a scaffold to bind synaptic proteins that regulate AZ structure. Alternatively, DYSC may act as the key interacting node via its PDZ domains in a SLO-dependent manner. Distinguishing between these (and other) possibilities will be a productive avenue of future research.

The morphological and physiological phenotypes observed in *dysc* and *slo* mutants may be mechanistically linked. Recent evidence suggests a causal link between spontaneous neurotransmission and synaptic bouton budding (Choi et al., 2014). Under genetic conditions where spontaneous neurotransmission is inhibited but evoked neurotransmission is maintained, hyper-budding of synaptic boutons is observed at the larval NMJ (Choi et al., 2014). Importantly, mutations in *complexin*, which result in extremely high frequencies of miniature events due to a loss of pre-fusion clamping of synaptic vesicles, exhibit increased synaptic bouton size (Choi et al., 2014; Huntwork and Littleton, 2007). The enhancement of spontaneous neurotransmission in *dysc* and *slo* mutants may therefore contribute to the enlargement of synaptic boutons in both mutant backgrounds.

In addition, alterations in the synaptic localization of cytoskeletal protein Futsch may also act to independently increase synaptic bouton size in *dysc* and *slo* mutants. Futsch is a microtubule-binding protein that is crucial for synaptic bouton budding (Roos et al., 2000); mutations resulting in loss of Futsch function or the mislocalization of Futsch inhibit correct synaptic bouton budding, resulting in synapses with a reduced number of aberrantly large boutons (Mosca et al., 2012; Pennetta et al., 2002; Roos et al., 2000). We therefore posit a causal role for Futsch in mediating the abnormal development of synaptic boutons that results from loss of DYSC and SLO. However, we cannot rule out the possibility that mislocalization Futsch merely correlates with increases in bouton size in *dysc* and *slo* mutants. Mutations in *futsch* do not affect AZ structure or increase spontaneous neurotransmission (Lepicard et al., 2014), suggesting the alterations in T-bar architecture and spontaneous vesicle release are not downstream of changes in synaptic Futsch localization, but represent parallel pathways by which DYSC and SLO influence synaptic development and physiology.

In conclusion, our research sheds new light on the roles of DYSC and its binding partner SLO in the *Drosophila* nervous system. The mammalian DYSC and SLO homologs whirlin and KCNMA1 may play similar roles in synaptic development and function.

MATERIALS AND METHODS

Drosophila genetics and molecular biology

Flies were reared on standard food containing cornmeal, yeast and molasses at 25°C under 12 h light:12 h dark cycles. The $dysc^{c03838}$ and $dysc^{s168}$ P-element insertions have been described previously (Jepson et al., 2012). The *elav*-Gal4 and *24B*-Gal4 stocks, flies harboring the slo^{11481} Minos element, a deficiency line that removes the *slo* locus [w^{1118}; +; *Df*(3R)BSC397] and the $dysc^{Mi02729}$ MiMIC insertion used to generate the *dysc::gfp* allele were obtained from the Bloomington Stock Center. To control for potential differences in genetic background, all *dysc* and *slo* alleles were outcrossed into a $white^{1118}$ (*iso*31) background for 5-10 generations prior to experimentation. The *dysc::gfp* allele was generated by ΦC31-mediated recombination between a construct containing the GFP/FlASH/StrepII/3×FLAG protein trap and an artificial MiMIC exon in the *dysc* locus ($dysc^{Mi02729}$), as described previously (Venken et al., 2011). Transgenic fly lines containing GFP/FlASH/StrepII/3×FLAG insertions were generated by standard germline transformation (Rainbow Transgenics). Fly head mRNA was extracted using TRIzol (Life Technologies), and reverse transcribed using High Capacity cDNA Reverse Transcriptase Kit (Applied Biosystems). See methods in the supplementary material for primer sequences used in this study.

Larval behavior

Third-instar wandering larvae were collected, gently rinsed in PBS and placed on 5% sucrose/2% agar plates. One larva was counted per plate, and the number of peristaltic body wall contractions was measured visually over a 1 min period under a dissecting microscope.

Confocal microscopy, immunohistochemistry and quantification of synaptic parameters

Wandering third instar larvae were used for confocal and STED imaging of larval synapses and AZs at muscle 6/7 or muscle 4 of segment 3. For all larval experiments, both sexes were used. Adult brains were dissected and immunostained as described previously (Wu and Luo, 2006). All confocal microscopy was performed using an Olympus Fluoview confocal microscope. Images were contrast enhanced in Adobe Photoshop. Where images of multiple genotypes are presented, all images were subject to the same enhancements. See methods in the supplementary material for further information on quantification of synaptic parameters, antibodies and staining protocols.

STED imaging

STED images were acquired on a Leica TCS SP5 STED CW microscope with a 100×1.4 NA oil objective. The Alexa 488 secondary antibody was excited with a 488 nm laser line and depleted by a 592 nm laser line. STED images were deconvolved using the built-in deconvolution algorithm of the Leica LAS-AF software (Signal Intensity filter, regulation parameter: 0.01-0.02). The point spread function was generated using a 2D Lorentz function with the full-width half-maximum set to 70 nm. AZ areas were measured blind with respect to the experimental genotype. Only individual AZs that could be clearly distinguished from other AZs were included in the area measurements.

Electrophysiology

Larvae were dissected and recorded in hemolymph-like saline HL3.1 containing (in mM): 70 NaCl, 5 KCl, 1 $CaCl_2$, 4 $MgCl_2$, 10 $NaHCO_3$, 5 trehalose, 115 sucrose and 5 HEPES (pH 7.2) as described previously (Feng et al., 2004; Ueda and Wu, 2006). The segmental nerves were severed from the ventral ganglion and stimulated with a suction electrode. Recordings were performed on ventral longitudinal muscle 6/7 in abdominal segments A3-A5 of third instar larvae. All cells selected for recording had resting membrane potentials between −50 and −70 mV. Both spontaneous and evoked postsynaptic currents were recorded while the muscle cell was voltage clamped at −60 mV, using an AxoClamp 2A (Axon Instruments) amplifier in single-electrode voltage clamp mode (switching frequency 10 KHz) and sharp microelectrodes (WPI) filled with 3 M KCl (5-10 MΩ resistance).

Acknowledgements

We thank Dr Nigel Atkinson and Bloomington and Harvard *Drosophila* stock centers for fly stocks; Dr Hugo Bellen and Dr Thomas Lloyd for technical advice; and Huihui Pan and Katelyn Kallas for technical assistance.

Competing interests

The authors declare no competing financial interests.

Author contributions

J.E.C.J., M.S., D.L., S.J.leM. and S.L. performed experiments. K.K., I.B.L., M.B.D. and M.N.W. supervised the work. J.E.C.J. and K.K. conceived the project and wrote the manuscript, with contributions from all authors.

Funding

This work was supported by the National Institutes of Health [GM088221 (to K.K.); DA022727, MH08642 and MH100093 (to M.B.D.); NS17910 (to I.B.L.), NS079584

(to M.N.W.)], by a grant from the Farber Family Foundation (I.B.L.) and by a Burroughs-Wellcome Fund Career Award for Medical Scientists (M.N.W.). Deposited in PMC for release after 12 months.

Supplementary material

Supplementary material available online at
http://dev.biologists.org/lookup/suppl/doi:10.1242/dev.109538/-/DC1

References

Atwood, H. L., Govind, C. K. and Wu, C.-F. (1993). Differential ultrastructure of synaptic terminals on ventral longitudinal abdominal muscles in *Drosophila* larvae. *J. Neurobiol.* **24**, 1008-1024.

Barrett, J. N., Magleby, K. L. and Pallotta, B. S. (1982). Properties of single calcium-activated potassium channels in cultured rat muscle. *J. Physiol.* **331**, 211-230.

Bean, B. P. (2007). The action potential in mammalian central neurons. *Nat. Rev. Neurosci.* **8**, 451-465.

Brown, M. R., Kronengold, J., Gazula, V.-R., Chen, Y., Strumbos, J. G., Sigworth, F. J., Navaratnam, D. and Kaczmarek, L. K. (2010). Fragile X mental retardation protein controls gating of the sodium-activated potassium channel Slack. *Nat. Neurosci.* **13**, 819-821.

Caroni, P., Donato, F. and Muller, D. (2012). Structural plasticity upon learning: regulation and functions. *Nat. Rev. Neurosci.* **13**, 478-490.

Chari, S. and Dworkin, I. (2013). The conditional nature of genetic interactions: the consequences of wild-type backgrounds on mutational interactions in a genome-wide modifier screen. *PLoS Genet.* **9**, e1003661.

Choi, B. J., Imlach, W. L., Jiao, W., Wolfram, V., Wu, Y., Grbic, M., Cela, C., Baines, R. A., Nitabach, M. N. and McCabe, B. D. (2014). Miniature neurotransmission regulates *Drosophila* synaptic structural maturation. *Neuron* **82**, 618-634.

Dworkin, I., Kennerly, E., Tack, D., Hutchinson, J., Brown, J., Mahaffey, J. and Gibson, G. (2009). Genomic consequences of background effects on scalloped mutant expressivity in the wing of *Drosophila melanogaster*. *Genetics* **181**, 1065-1076.

Dyba, M., Jakobs, S. and Hell, S. W. (2003). Immunofluorescence stimulated emission depletion microscopy. *Nat. Biotechnol.* **21**, 1303-1304.

Emes, R. D. and Grant, S. G. N. (2012). Evolution of synapse complexity and diversity. *Annu. Rev. Neurosci.* **35**, 111-131.

Ermolyuk, Y. S., Alder, F. G., Surges, R., Pavlov, I. Y., Timofeeva, Y., Kullmann, D. M. and Volynski, K. E. (2013). Differential triggering of spontaneous glutamate release by P/Q-, N- and R-type Ca^{2+} channels. *Nat. Neurosci.* **16**, 1754-1763.

Feng, Y., Ueda, A. and Wu, C.-F. (2004). A modified minimal hemolymph-like solution, HL3.1, for physiological recordings at the neuromuscular junctions of normal and mutant *Drosophila* larvae. *J. Neurogenet.* **18**, 377-402.

Frank, C. A., Kennedy, M. J., Goold, C. P., Marek, K. W. and Davis, G. W. (2006). Mechanisms underlying the rapid induction and sustained expression of synaptic homeostasis. *Neuron* **52**, 663-677.

Ghezzi, A., Al-Hasan, Y. M., Larios, L. E., Bohm, R. A. and Atkinson, N. S. (2004). slo K(+) channel gene regulation mediates rapid drug tolerance. *Proc. Natl. Acad. Sci. USA* **101**, 17276-17281.

Green, J. A., Yang, J., Grati, M., Kachar, B. and Bhat, M. A. (2013). Whirlin, a cytoskeletal scaffolding protein, stabilizes the paranodal region and axonal cytoskeleton in myelinated axons. *BMC Neurosci.* **14**, 96.

Holderith, N., Lorincz, A., Katona, G., Rózsa, B., Kulik, A., Watanabe, M. and Nusser, Z. (2012). Release probability of hippocampal glutamatergic terminals scales with the size of the active zone. *Nat. Neurosci.* **15**, 988-997.

Hu, H., Shao, L. R., Chavoshy, S., Gu, N., Trieb, M., Behrens, R., Laake, P., Pongs, O., Knaus, H. G., Ottersen, O. P. et al. (2001). Presynaptic Ca2+-activated K+ channels in glutamatergic hippocampal terminals and their role in spike repolarization and regulation of transmitter release. *J. Neurosci.* **21**, 9585-9597.

Huntwork, S. and Littleton, J. T. (2007). A complexin fusion clamp regulates spontaneous neurotransmitter release and synaptic growth. *Nat. Neurosci.* **10**, 1235-1237.

Jepson, J. E. C., Shahidullah, M., Lamaze, A., Peterson, D., Pan, H. and Koh, K. (2012). *dyschronic*, a *Drosophila* homolog of a deaf-blindness gene, regulates circadian output and Slowpoke channels. *PLoS Genet.* **8**, e1002671.

Johnson, E. L., III, Fetter, R. D. and Davis, G. W. (2009). Negative regulation of active zone assembly by a newly identified SR protein kinase. *PLoS Biol.* **7**, e1000193.

Katz, B. and Miledi, R. (1963). A study of spontaneous miniature potentials in spinal motoneurones. *J. Physiol.* **168**, 389-422.

Kaufmann, N., DeProto, J., Ranjan, R., Wan, H. and Van Vactor, D. (2002). *Drosophila* liprin-alpha and the receptor phosphatase Dlar control synapse morphogenesis. *Neuron* **34**, 27-38.

Kittel, R. J., Wichmann, C., Rasse, T. M., Fouquet, W., Schmidt, M., Schmid, A., Wagh, D. A., Pawlu, C., Kellner, R. R., Willig, K. I. et al. (2006). Bruchpilot promotes active zone assembly, Ca2+ channel clustering, and vesicle release. *Science* **312**, 1051-1054.

Koenig, J. H. and Ikeda, K. (1999). Contribution of active zone subpopulation of vesicles to evoked and spontaneous release. *J. Neurophysiol.* **81**, 1495-1505.

Lee, U. S. and Cui, J. (2010). BK channel activation: structural and functional insights. *Trends Neurosci.* **33**, 415-423.

Lee, J. and Wu, C.-F. (2010). Orchestration of stepwise synaptic growth by K+ and Ca2+ channels in *Drosophila*. *J. Neurosci.* **30**, 15821-15833.

Lee, J., Ueda, A. and Wu, C.-F. (2008). Pre- and post-synaptic mechanisms of synaptic strength homeostasis revealed by slowpoke and shaker K+ channel mutations in *Drosophila*. *Neuroscience* **154**, 1283-1296.

Lee, J., Ueda, A. and Wu, C.-F. (2014). Distinct roles of *Drosophila* cacophony and Dmca1D Ca(2+) channels in synaptic homeostasis: genetic interactions with slowpoke Ca(2+) -activated BK channels in presynaptic excitability and postsynaptic response. *Dev. Neurobiol.* **74**, 1-15.

Lepicard, S., Franco, B., de Bock, F. and Parmentier, M.-L. (2014). A presynaptic role of microtubule-associated protein 1/Futsch in *Drosophila*: regulation of active zone number and neurotransmitter release. *J. Neurosci.* **34**, 6759-6771.

Li, J., Ashley, J., Budnik, V. and Bhat, M. A. (2007). Crucial role of *Drosophila* neurexin in proper active zone apposition to postsynaptic densities, synaptic growth, and synaptic transmission. *Neuron* **55**, 741-755.

Liu, K. S. Y., Siebert, M., Mertel, S., Knoche, E., Wegener, S., Wichmann, C., Matkovic, T., Muhammad, K., Depner, H., Mettke, C. et al. (2011). RIM-binding protein, a central part of the active zone, is essential for neurotransmitter release. *Science* **334**, 1565-1569.

Matz, J., Gilyan, A., Kolar, A., McCarvill, T. and Krueger, S. R. (2010). Rapid structural alterations of the active zone lead to sustained changes in neurotransmitter release. *Proc. Natl. Acad. Sci. USA* **107**, 8836-8841.

Mburu, P., Mustapha, M., Varela, A., Weil, D., El-Amraoui, A., Holme, R. H., Rump, A., Hardisty, R. E., Blanchard, S., Coimbra, R. S. et al. (2003). Defects in whirlin, a PDZ domain molecule involved in stereocilia elongation, cause deafness in the whirler mouse and families with DFNB31. *Nat. Genet.* **34**, 421-428.

McKiernan, E. C. (2013). Effects of manipulating slowpoke calcium-dependent potassium channel expression on rhythmic locomotor activity in *Drosophila* larvae. *PeerJ* **1**, e57.

Mosca, T. J., Hong, W., Dani, V. S., Favaloro, V. and Luo, L. (2012). Trans-synaptic Teneurin signalling in neuromuscular synapse organization and target choice. *Nature* **484**, 237-241.

Müller, M. and Davis, G. W. (2012). Transsynaptic control of presynaptic Ca(2)(+) influx achieves homeostatic potentiation of neurotransmitter release. *Curr. Biol.* **22**, 1102-1108.

Nieratschker, V., Schubert, A., Jauch, M., Bock, N., Bucher, D., Dippacher, S., Krohne, G., Asan, E., Buchner, S. and Buchner, E. (2009). Bruchpilot in ribbon-like axonal agglomerates, behavioral defects, and early death in SRPK79D kinase mutants of *Drosophila*. *PLoS Genet.* **5**, e1000700.

Owald, D., Khorramshahi, O., Gupta, V. K., Banovic, D., Depner, H., Fouquet, W., Wichmann, C., Mertel, S., Eimer, S., Reynolds, E. et al. (2012). Cooperation of Syd-1 with Neurexin synchronizes pre- with postsynaptic assembly. *Nat. Neurosci.* **15**, 1219-1226.

Parrish, J. Z., Kim, C. C., Tang, L., Bergquist, S., Wang, T., Derisi, J. L., Jan, L. Y., Jan, Y. N. and Davis, G. W. (2014). Kruppel mediates the selective rebalancing of ion channel expression. *Neuron* **82**, 537-544.

Pennetta, G., Hiesinger, P. R., Fabian-Fine, R., Meinertzhagen, I. A. and Bellen, H. J. (2002). *Drosophila* VAP-33A directs bouton formation at neuromuscular junctions in a dosage-dependent manner. *Neuron* **35**, 291-306.

Ping, Y. and Tsunoda, S. (2012). Inactivity-induced increase in nAChRs upregulates Shal K(+) channels to stabilize synaptic potentials. *Nat. Neurosci.* **15**, 90-97.

Prakriya, M. and Lingle, C. J. (1999). BK channel activation by brief depolarizations requires Ca2+ influx through L- and Q-type Ca2+ channels in rat chromaffin cells. *J. Neurophysiol.* **81**, 2267-2278.

Reist, N. E., Buchanan, J., Li, J., DiAntonio, A., Buxton, E. M. and Schwarz, T. L. (1998). Morphologically docked synaptic vesicles are reduced in synaptotagmin mutants of *Drosophila*. *J. Neurosci.* **18**, 7662-7673.

Roos, J., Hummel, T., Ng, N., Klämbt, C. and Davis, G. W. (2000). *Drosophila* Futsch regulates synaptic microtubule organization and is necessary for synaptic growth. *Neuron* **26**, 371-382.

Sigrist, S. J. and Schmitz, D. (2011). Structural and functional plasticity of the cytoplasmic active zone. *Curr. Opin. Neurobiol.* **21**, 144-150.

Sone, M., Suzuki, E., Hoshino, M., Hou, D., Kuromi, H., Fukata, M., Kuroda, S., Kaibuchi, K., Nabeshima, Y. and Hama, C. (2000). Synaptic development is controlled in the periactive zones of *Drosophila* synapses. *Development* **127**, 4157-4168.

Südhof, T. C. (2008). Neuroligins and neurexins link synaptic function to cognitive disease. *Nature* **455**, 903-911.

Ueda, A. and Wu, C.-F. (2006). Distinct frequency-dependent regulation of nerve terminal excitability and synaptic transmission by IA and IK potassium channels revealed by *Drosophila* Shaker and Shab mutations. *J. Neurosci.* **26**, 6238-6248.

Development (2014) 141, 4548-4557 doi:10.1242/dev.109538

Venken, K. J. T., Schulze, K. L., Haelterman, N. A., Pan, H., He, Y., Evans-Holm, M., Carlson, J. W., Levis, R. W., Spradling, A. C., Hoskins, R. A. et al. (2011). MiMIC: a highly versatile transposon insertion resource for engineering *Drosophila melanogaster* genes. *Nat. Methods* **8**, 737-743.

Verpelli, C., Schmeisser, M. J., Sala, C. and Boeckers, T. M. (2012). Scaffold proteins at the postsynaptic density. *Adv. Exp. Med. Biol.* **970**, 29-61.

Wagh, D. A., Rasse, T. M., Asan, E., Hofbauer, A., Schwenkert, I., Dürrbeck, H., Buchner, S., Dabauvalle, M.-C., Schmidt, M., Qin, G. et al. (2006). Bruchpilot, a protein with homology to ELKS/CAST, is required for structural integrity and function of synaptic active zones in *Drosophila*. *Neuron* **49**, 833-844.

Wang, A. D., Sharp, N. P. and Agrawal, A. F. (2014). Sensitivity of the distribution of mutational fitness effects to environment, genetic background, and adaptedness: a case study with *Drosophila*. *Evolution* **68**, 840-853.

Wichmann, C. and Sigrist, S. J. (2010). The active zone T-bar: a plasticity module? *J. Neurogenet.* **24**, 133-145.

Wojtowicz, J. M., Marin, L. and Atwood, H. L. (1994). Activity-induced changes in synaptic release sites at the crayfish neuromuscular junction. *J. Neurosci.* **14**, 3688-3703.

Wondolowski, J. and Dickman, D. (2013). Emerging links between homeostatic synaptic plasticity and neurological disease. *Front. Cell. Neurosci.* **7**, 223.

Wu, J. S. and Luo, L. (2006). A protocol for dissecting *Drosophila melanogaster* brains for live imaging or immunostaining. *Nat. Protoc.* **1**, 2110-2115.

Zhang, Y., Brown, M. R., Hyland, C., Chen, Y., Kronengold, J., Fleming, M. R., Kohn, A. B., Moroz, L. L. and Kaczmarek, L. K. (2012). Regulation of neuronal excitability by interaction of fragile X mental retardation protein with slack potassium channels. *J. Neurosci.* **32**, 15318-15327.